

RESEARCH ARTICLE

Joint vehicle state and parameters estimation via Twin-in-the-Loop observers

F. Dettù^a, S. Formentin^a and S. M. Savaresi^a

^aDipartimento di Elettronica, Informazione e Bioingegneria, Politecnico di Milano, Piazza Leonardo da Vinci 32, 20133, Milano, Italy.

ARTICLE HISTORY

Compiled December 13, 2023

Abstract

Vehicular control systems are required to be both extremely reliable and robust to different environmental conditions, *e.g.* load or tire-road friction. In this paper, we extend a new paradigm for state estimation, called Twin-in-the-Loop filtering (TiL-F), to the estimation of the unknown parameters describing the vehicle operating conditions. In such an approach, a digital-twin of the vehicle (usually already available to the car manufacturer) is employed on-board as a plant replica within a closed-loop scheme, and the observer gains are tuned purely from experimental data. The proposed approach is validated against experimental data, showing to significantly outperform the state-of-the-art solutions.

KEYWORDS

Parameter estimation; state estimation; driving simulator; sensors; signal processing.

1. Introduction

The *Twin-in-the-Loop* (TiL) framework has been recently proposed for vehicle dynamics control [2] and estimation of unknown states and variables [13]. In this innovative framework, an high-fidelity off-the-shelf vehicle dynamics simulator is employed in a control/estimation loop - thanks to the recent developments in on-board hardware platforms¹. Being the simulator a commercial product, we assume it to be a black-box, *i.e.* we can only extract its outputs given some inputs, but we are not able to access its equations and update rules directly. With regards to the TiL estimator, the authors in [13] showed how the presented algorithm is able to estimate both unmeasured states (*e.g.* vehicle sideslip) and other unknown variables, such as the tire-road forces. However, they did not address the estimation of time-varying parameters; in fact, modern vehicle dynamics controllers are strongly based on time-domain models of the process [9,18,19]. Due to the variability of conditions during the daily use of a vehicle - *e.g.* the most common case being the payload - such controllers can underperform, or even destabilize the system, if such variations are not properly addressed. Hence, following a well established research trend on vehicle state and parameters estimation, we build

CONTACT F. Dettù, email: federico.dettu@polimi.it. S. Formentin, email: simone.formentin@polimi.it. S. M. Savaresi, email: sergio.savaresi@polimi.it.

¹For example, <https://www.vi-grade.com/en/products/autohawk/>.

this research within the TiL framework, extending it to a new application.

Related works. Existing literature solutions for four-wheeled vehicles on-line parameter estimation can be broadly split among direct sensing and software sensing ones. In the first class of solutions, a sensor for the measurement of the variable of interest is used (*e.g.* [26], where the mass is estimated via strain gauges on the suspensions). The second class of solutions features instead the estimation of unmeasurable variables via production available sensors (*i.e.* without adding new piece of hardware). If we focus on software sensing algorithms, we find many solutions in the literature - where we cite here the most relevant contributions in the past years - [6,7,12,14,15,24,25,27], which can be categorized according to four axes: estimated quantities, employed sensors, used estimation algorithm, and employed model. Other important contributions design software sensing with an highly specific goal, like rollover risk evaluation [23]: we do not consider them in this review.

On the estimated quantities side, the mass M is indeed the most important vehicle parameter, and is always considered in the cited works; vehicle yaw inertia J_{zz} is then considered in [7,24,25], while roll and pitch inertia J_{xx} , J_{yy} are considered in [15]. Other estimated parameters include longitudinal [7,15,24], lateral [15] or vertical [23] center-of-mass position variation. The tire-road friction coefficient is estimated in [14] - however, this parameter is different in nature from the other considered in the literature, as its variations are not imputable to a variation of the vehicle load conditions, but rather to the terrain.

With regards to the sensing layout, one common denominator is the use of classical production vehicle sensors, like gyroscopes or Inertial Measurement Units (IMU); yaw rate, which is a gyroscope output, is employed in all the cited articles but [15]. Acceleration information is used in all references; [15] use three acceleration sensors, to be placed above the unsprung masses. Other considered sensors include wheel angular speed [14,27], suspension displacement [14], GPS position measurements [14] and vehicle longitudinal speed [7,24,25].

Moving further to the considered estimation algorithm, most works are based on Kalman Filtering (KF) [7,12,14,24,25], specifically declined - except for [12,14,25] - in its *Dual* formulation; *Dual* KF is based on two separated observers, one devoted to classical state filtering, and the other one solely devoted to parameter estimation, to be switched-off once a good estimate of said parameters has been reached. [27] propose a similar formulation, where the correction law is computed via a particle filter. On the other hand, [15] propose a different approach, based on the use of free decay responses of the vehicle - more similar to a classic identification algorithm rather than to a state observer.

Finally, when coming to employed plant replica, the simplest model is the single-track, which is however only used in [12], as it fails to capture most of vehicle dynamics non-linearities. The most common model is the double-track [7,12,24,25,27]; the latter can be enhanced with roll dynamics, as in [7,24], or wheel dynamics [27], depending on the estimation target or the available measurements. [15] consider a full vehicle model - *i.e.* featuring also unsprung mass dynamics, roll and pitch dynamics. Finally, the most complex model is the one proposed in [14]: the authors consider a multibody model - featuring 14 states.

Contributions. From the literature review, an important point emerges. As also pointed out in [13], classical vehicular state observers are based on simplified models of the variables to be estimated: an ad-hoc model for each variable is required, and each model has to be accurately calibrated. Given that approximately 75% of the

time of a control system design project is devoted to modelling, as indicated in [4], the resulting procedure turns out to be cumbersome. Let this apart, consider that any estimator is based upon a set of hyperparameters controlling its behaviour - *e.g.* the noise covariances in Kalman Filters. Generally speaking, the more complex an estimator is, the longer the hyperparameter selection is. Relying on simple correction laws is thus beneficial in the implementation phase.

In TiL framework we employ a single model - a digital twin - for each variable to be estimated: this solves the problem of designing ad-hoc models and of having many models running at run-time on the same estimation algorithm. The model calibration phase comes for free when using a digital twin, in the assumption that a car manufacturer already has a library of simulators for their production vehicles. On the other hand, the correction algorithm complexity is now shifted to the model fidelity: the more faithful to the real system the model is, the less intense - and thus simple - the correction need to be. The authors in [13] actually show as a linear and time-invariant correction law is sufficient to outperform the benchmark.

Matter-of-factly, the authors in [14] consider an high-fidelity model of the plant as in TiL framework: however, being the considered model a white-box, the authors are able to directly compute the update rules via a Kalman Filter-like algorithm. This is not possible in TiL, as the underlying model is a black-box, and the correction law, although linear, has to be tuned via model-free approaches [13].

With respect to the research in [13], we extend the TiL framework to the estimation of varying parameters, providing insights on how the correction law has to be designed, and on the feasibility of the approach in terms of robustness to measurement noise and uncertainty.

The paper is structured as follows. In Section 2 we provide to the reader some preliminaries on the TiL estimator. Section 3 defines the problem of varying mass and moment of inertia, and its estimation. Then, in Section 4 we conduct an in-depth analysis of the parameters estimation problem by independently considering set of variables, providing sensitivity analyses to uncertainty and noise. Section 5 shows an application of the described and simulated framework on experimental data, while Section 6 concludes the manuscript with a few considerations.

2. Twin-in-the-Loop observer architecture

[13] proposed an unified estimator for all the variables of interest in vehicle dynamics control. In such an architecture (see Fig. 1), the two main features are the following

- The vehicle simulator, an high-fidelity plant replica, whose equations are a black-box.
- The closed-loop correction, based upon available measurements, perturbs the model in order to properly estimate unknown variables.

The detailed architecture of the complete observer is given in Fig. 2. Generically speaking, the simulator states at time k are updated according to the following equations

$$\begin{aligned}\tilde{x}_{k+1} &= f(\hat{x}_k, u_k, \tilde{z}_k, p), \\ \tilde{y}_k &= g(\hat{x}_k, u_k, \tilde{z}_k, p), \\ \tilde{z}_k &= h(\hat{x}_k, u_k, \delta\hat{z}_{k-1}, p)\end{aligned}\tag{1}$$

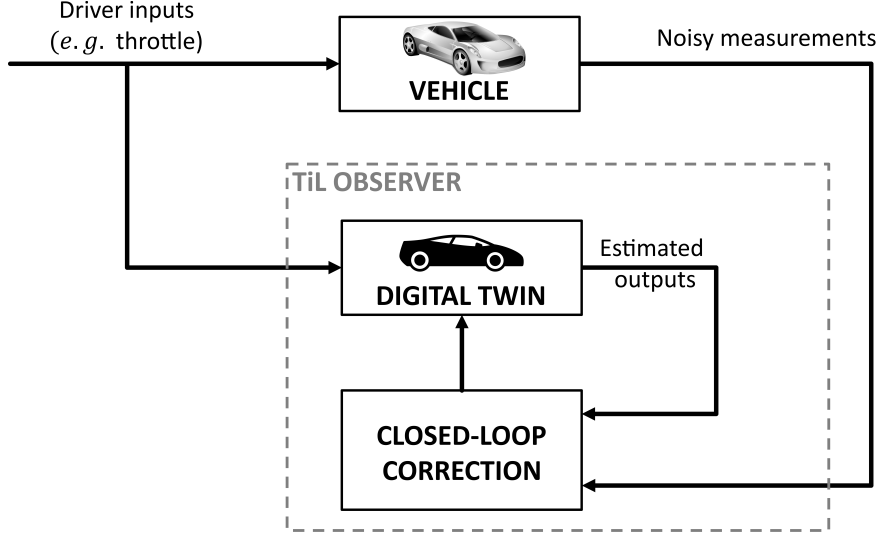


Figure 1. Twin-in-the-Loop estimation scheme.

where f , g , h are unknown (possibly nonlinear) functions, $y \in \mathbb{R}^{n_y}$ is the set of measurable outputs, $x \in \mathbb{R}^{n_x}$ is the set of internal states of the simulator, $z \in \mathbb{R}^{n_z}$ is a set of additional variables to be estimated and p is a set of constant parameters. We denote $\tilde{\nu}_k$ an a-priori estimation for a certain variable ν_k : then closed-loop correction updates the a-priori estimates, and generates a-posteriori ones $\hat{\nu}_k$ - as in the widely known Kalman Filter formulation.

The authors in [13] extend the state vector to estimate tire-road contact forces; more specifically, the additional variables z are estimated by correcting the nominal values provided by the simulator

$$\hat{z}_k = \tilde{z}_k + \delta \hat{z}_k. \quad (2)$$

The artificial variable $\delta \hat{z}_k$ is described by a fictitious constant dynamics equation

$$\delta \tilde{z}_{k+1} = \delta \hat{z}_k. \quad (3)$$

The latter assumption is widely used in case the parameters to be estimated are slowly varying. Overall, the set of states, including internal and extended ones, now reads $x^{aug} = [x^T \ \delta z^T]^T$. At this point, the innovation term at step k , consisting in the mismatch among measured (y_k) and a-priori estimated outputs (\tilde{y}_k) is to be used to correct the state vector x^{aug} . The innovation is mapped onto the states via a linear law in [13]

$$\begin{aligned} \Delta x_k^{aug} &= K (y_k - \tilde{y}_k) \\ \hat{x}_k^{aug} &= \tilde{x}_k^{aug} + \Delta x_k^{aug}. \end{aligned} \quad (4)$$

However, we will show in the following that the linear formulation is inadequate for the estimation of certain parameters, *e.g.* the vehicle mass or inertia. Let us thus define a

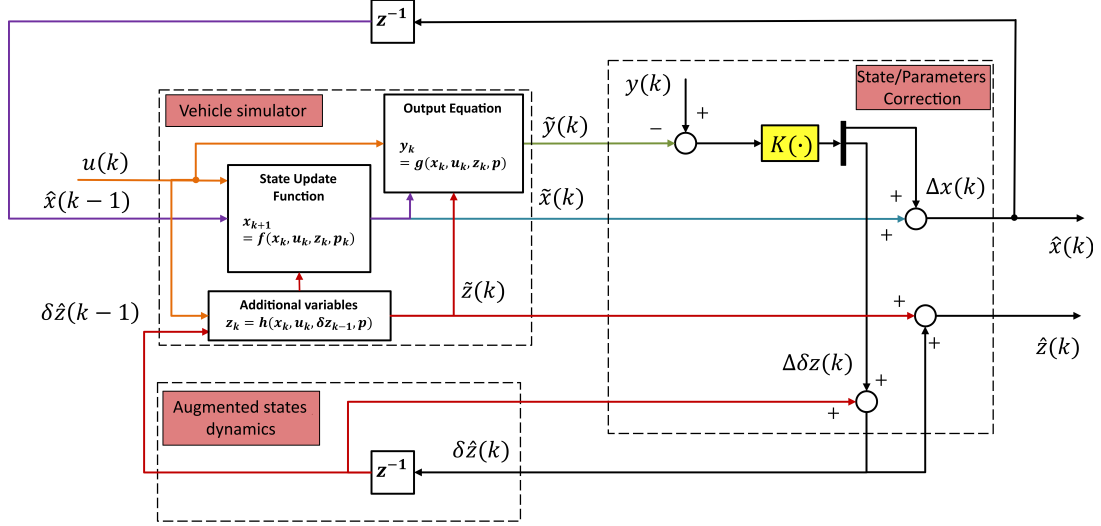


Figure 2. Twin-in-the-Loop complete estimation architecture, featuring correction of simulator states and augmented states.

mixed linear-nonlinear correction law

$$\hat{x}_k^{aug} = \tilde{x}_k^{aug} + \begin{bmatrix} K & 0 \\ 0 & \mathcal{K}(y_k) \end{bmatrix} (y_k - \tilde{y}_k), \quad (5)$$

where $K \in \mathbb{R}^{n_x \times n_y}$ maps the innovation onto the nominal states, and $\mathcal{K}(y_k) \in \mathbb{R}^{n_z \times n_y}$ maps the innovation onto the extended states.

3. A parameter estimation case study: the uncertain load setting

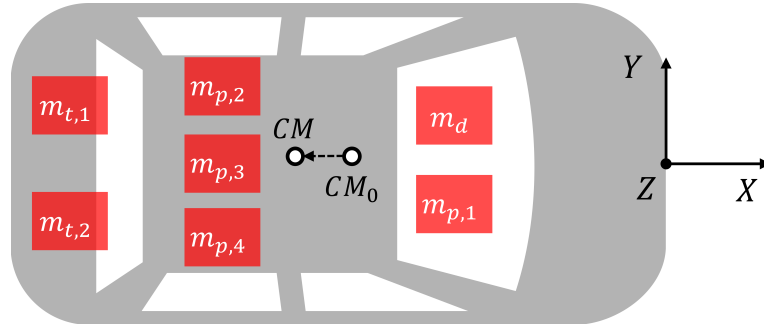


Figure 3. Vehicle top view, considering differently added additional masses.

Among the physical parameters defining a vehicle, mass and inertia might significantly change due to different load conditions, while being extremely important in several on-board control systems. Hence, we consider in the following the problem of estimating such parameters in a road vehicle via the TiL estimator architecture. Consider the 5-seats vehicle in Fig. 3. Such vehicle can be loaded with additional masses. On the mathematical perspective, we assume each of the m_i , $i = 1, \dots, \mathcal{M}$ to be a

point mass, characterized by a certain position $p_{m_i} = (p_{m_i,x}, p_{m_i,y}, p_{m_i,z})$ in the reference frame defined by axes X, Y, Z - as displayed in Fig. 3. If we assume that the vehicle chassis can be modeled as a rigid body with its mass concentrated in a single point - a common assumption in vehicle dynamics - the center-of-mass of such system is computed as [20]

$$\begin{aligned} CM_x &= \sum_{i=0,\dots,\mathcal{M}} m_i \cdot p_{m_i,x}, \\ CM_y &= \sum_{i=0,\dots,\mathcal{M}} m_i \cdot p_{m_i,y}, \\ CM_z &= \sum_{i=0,\dots,\mathcal{M}} m_i \cdot p_{m_i,z}. \end{aligned} \quad (6)$$

whereas m_0 denotes the original lumped mass of the chassis. Indeed, the center-of-mass including additional masses - $CM = (d_x, d_y, d_z)$ - is going to be different from the original one - $CM_0 = (d_{0,x}, d_{0,y}, d_{0,z})$. The new lumped mass is then simply defined as

$$M_{tot} = m_0 + \sum_{i=1,\dots,\mathcal{M}} m_i. \quad (7)$$

Consequently, the chassis moments and products of inertia change due to the mass variation and the re-defined center-of-mass [20]. Considering the Huygens-Steiner theorem [5], we obtain the new moments/products of inertia, defined with respect to CM ; this is done starting from the ones defined in CM_0 and taking into account the newly added masses. *E.g.*, for the moments of inertia - J_{xx}, J_{yy}, J_{zz} - one has

$$\begin{aligned} J_{xx} &= J_{xx,0} - m_0 [\delta(d_y, d_{y,0}) + \delta(d_z, d_{z,0})] + \\ &\quad \sum_{i=1,\dots,\mathcal{M}} m_i [\delta(p_{m_i,y}, d_y) + \delta(p_{m_i,z}, d_z)], \\ J_{yy} &= J_{yy,0} - m_0 [\delta(d_x, d_{x,0}) + \delta(d_z, d_{z,0})] + \\ &\quad \sum_{i=1,\dots,\mathcal{M}} m_i [\delta(p_{m_i,x}, d_x) + \delta(p_{m_i,z}, d_z)], \\ J_{zz} &= J_{zz,0} - m_0 [\delta(d_x, d_{x,0}) + \delta(d_y, d_{y,0})] + \\ &\quad \sum_{i=1,\dots,\mathcal{M}} m_i [\delta(p_{m_i,x}, d_x) + \delta(p_{m_i,y}, d_y)], \end{aligned} \quad (8)$$

whereas $J_{xx,0}, J_{yy,0}, J_{zz,0}$ represent the chassis nominal moment of inertia, and $\delta(x_1, x_2) = (x_1 - x_2)^2$. Also product of inertia variations - *e.g.* J_{xy} - can be quantified analytically in a similar way; for the load conditions considered in the case study - realistic ones for road vehicles - we don't have significant variations of these parameters.

Now, let us consider again scheme of Fig. 1: the high-fidelity digital twin is modelled with a set of nominal parameters, *i.e.* lumped mass, inertia, and center-of-mass location. The real vehicle is instead loaded with additional masses, and thus "perturbed" from the nominal parameters set.

In [13], the authors design a closed-loop correction so as to force the simulator states to be identical to the ones of the real vehicle, regardless of the reasons leading to

differences between the two instances of the vehicle. On the other hand, in the present work we shift the philosophy, trying to estimate also the exact differences among the two instances.

4. Simulation analysis

Nominal param.	Value
m_0 [kg]	2125.8
$J_{xx,0}$ [kg · m ²]	834.23
$J_{yy,0}$ [kg · m ²]	3640.182
$J_{zz,0}$ [kg · m ²]	3932.77
$J_{xy,0}$ [kg · m ²]	0.14
$J_{xz,0}$ [kg · m ²]	0.097
$J_{yz,0}$ [kg · m ²]	3.86
$d_{0,x}$ [cm]	-125.0
$d_{0,y}$ [cm]	-0.003
$d_{0,z}$ [cm]	64.4

Table 1. Nominal vehicle mass, inertia and CM parameters.

Additional load param.	Value
$m_{p,1}$ [kg]	75 kg
$m_{p,2}$ [kg]	80 kg
$m_{p,3}$ [kg]	65 kg
$m_{p,4}$ [kg]	75 kg
$m_{t,1}$ [kg]	30 kg
$m_{t,2}$ [kg]	30 kg

Table 2. Additional load parameters.

In this Section, we demonstrate the TiL methodology for the case study of Section 3. For a better assessment of the potentialities and limitations of the present method, we conduct a preliminary analysis in a controlled simulation environment. The nominal chassis parameters of the considered vehicle are given in Table 1. Said nominal parameters also include the presence of a driver (m_d in Fig. 3). The parameters are those of a generic sport utility vehicle, which is modeled in VI-CarRealTime (CRT) simulation environment [21]. The nominal vehicle model is perturbed by adding masses according to the scheme of Fig. 3; the values of such loads are given in Table 2. For this new configuration, the center-of-mass, mass and inertia can be analytically computed according to what described in Section 3; the new values for the most relevant parameters are in Table 3.

We apply the TiL architecture to the problem herein, defining the complete extended

Perturbed param.	Value	Variation ²
M_{tot} [kg]	2480.8	+16.70 %
J_{xx} [kg · m ²]	901.9	+8.11 %
J_{yy} [kg · m ²]	4394.4	+20.72 %
J_{zz} [kg · m ²]	4760.0	+21.03 %
d_x [cm]	-131.6	+5 %
d_y [cm]	1.6	+100.2 %
d_z [cm]	68.4	+5.3 %

Table 3. Perturbed vehicle parameters.

state vector as

$$x^{aug} = [x^T \quad \delta M \quad \delta J_{xx} \quad \delta J_{yy} \quad \delta J_{zz}]^T, \quad (9)$$

where x is the set of VI-CarRealTime states, $x \in R$. In this simulation analysis, only extended states - parameters - are going to be corrected, as we want to focus on the feasibility of parameters correction. Each extended state represents the deviation of said parameter from the nominal value provided by the simulator as an output. Joint state and parameter correction will be considered in an experimental case study in Section 5.

In order to reproduce a simulation environment the closer to a real scenario, we introduce measurement noise. The noise is introduced on the signals coming from an - simulated in CRT - inertial measurement unit (IMU) placed near the vehicle CM. The following noise law is considered

$$s_n = s + n_s, \quad n_s \sim WN(0, \sigma_s^2), \quad (10)$$

where s is a signal coming from an IMU, and σ_s is the standard deviation of a suitable white noise. In the simulation case study, x -axis acceleration a_x and x , y , z axes angular rates $\omega_{x,y,z}$ are employed as measurements in the observer, hence, only these signals are perturbed with noise. When not specified, the snr is tuned to be ≈ 10 : however, we also conduct sensitivity analyses to verify the impact of measurement noise onto the estimator.

When quantifying the observer performance, we consider as a metric the root mean square estimation error in the last $w = 1$ seconds of test, as the dynamics of the estimated parameters are rather slow, and considering larger windows would take into account transient effects.

$$rms_v = \frac{1}{wf_s} \sum_{k=N_s-wf_s}^{N_s} (\nu_k - \hat{\nu}_k)^2, \quad (11)$$

Where N_s is the number of samples in an experiment, $f_s [Hz]$ is the sampling frequency, and ν is a suitable parameter or variable to be estimated, *e.g.* $\nu = \delta M$.

On the other hand, we also consider the percentage version of rms_w , in order to quantify the amount of error within the parameters values. This metric is defined as

$$rms_{\nu, \%} = rms_{\nu} / \nu_0, \quad (12)$$

Where ν_0 is the nominal value of a variable to be estimated; *e.g.* in our case, the nominal value for δM is the difference among the perturbed value in Table 3 and the nominal value in Table 1.

In the following, we consider as acceptable a percentage rms smaller than the 10 % of a perturbed variable.

4.1. Center-of-mass position identification

The CM position is perturbed from CM_0 in the modified layout, as evident from Table 3. Most significant displacement occur along x and z axes, as y axis variation are mostly due to extremely unbalanced - on the left-right direction - loads, which are

not common in road vehicles. Given that the digital twin computes the torque and force balances referring to the center-of-mass, a not exact knowledge of CM might be detrimental for estimating the other parameters.

Two possible ways of solving this problem exist:

- Insert the variables d_x , d_y , d_z onto the augmented state vector x^{aug} , and consequently correct the mismatch from the nominal values;
- Identify in a traditional way - see *e.g.* [8,17] - d_x , d_y , d_z on-line via available data and simplified models.

In the present work, we decide to follow the second approach, as we want to concentrate onto the estimation of mass and inertia: hence, we assume correct knowledge of CM . However, we also perform sensitivity analyses to check the effect of a wrong CM onto the estimation performance: in general, we will show as for the considered load conditions, which are reasonable for a passenger car, the performance loss is negligible even in case of wrong CM estimation.

4.2. Vehicle mass estimation

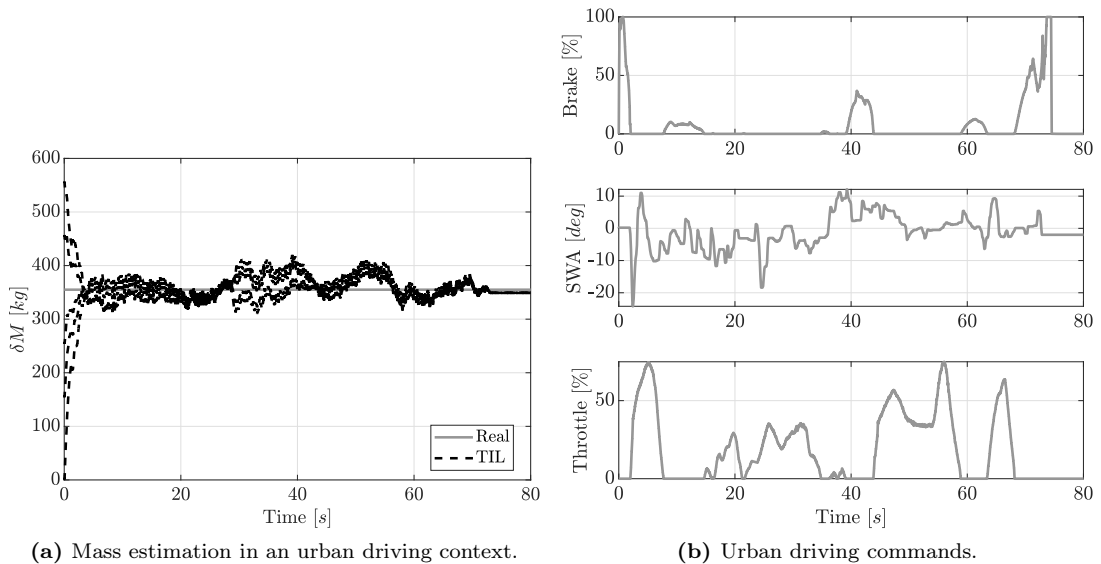


Figure 4. Mass estimation in an urban driving like context, with noisy measurements. Estimated mass for different initial conditions.

Vehicle chassis mass can be estimated by suitably exciting the longitudinal dynamics. Consider the following simplified longitudinal dynamics balance for a road vehicle

$$M_{chassis} \cdot a_x = F_{trac} - F_{brake} - F_{roll} - F_{aero}. \quad (13)$$

It is clear that, provided that roughly the same forces act on the vehicle, an increased mass yields a lower longitudinal acceleration. Hence, if the digital twin is characterized by a smaller mass than the real vehicle, a suitable correction can be based upon the difference between longitudinal accelerations. Indeed, if the terms on the right hand side of Eq. (13) are significantly different, we are not able to determine whether an

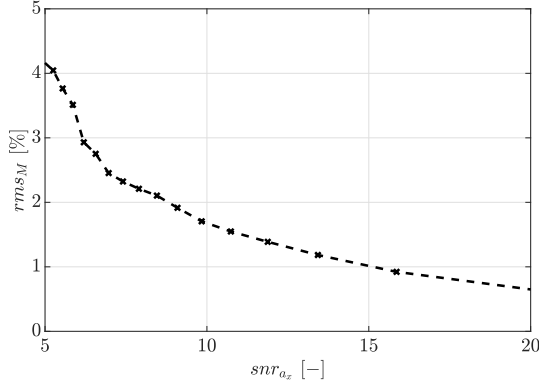


Figure 5. Mass estimation with varying noise levels.

Test conditions	rms_M [%]
<ul style="list-style-type: none"> • Noiseless data ($snr = \infty$); • Correct CM 	0.64
<ul style="list-style-type: none"> • Noisy data ($snr = 10$); • Correct CM. 	1.61
<ul style="list-style-type: none"> • Noisy data ($snr = 10$); • Wrong CM. 	0.68

Table 4. Mass estimation performance in different conditions.

acceleration variation is due to a mass difference or rather to an error in modelling the brake system or the tire-road interaction. For this reason, in this simulation analysis the sole modelling difference among the two simulated instances of the vehicle lie in the mass perturbation. In Section 5 we will test the mass estimation on real data, where other modelling differences might exist.

The correction applied on δM at time step k reads

$$\Delta \delta M_k = K_{a_x - \delta M} \cdot \text{sgn}(a_{x,k}) \cdot (a_{x,k} - \tilde{a}_{x,k}), \quad (14)$$

Where $K_{a_x, \delta M}$ is a suitable gain to be tuned and $\text{sgn}(\cdot)$ extracts the sign of the argument. Note as $\mathcal{K}(y_k) = K_{a_x - \delta M} \cdot \text{sgn}(a_{x,k})$ in this context.

The importance of the sign operator is easily understood with a simple example. Consider a coasting down - deceleration due to inertia $a_x < 0$ - event: if the vehicle has an higher mass than the simulator, it will coast down faster, thus $(a_x - \tilde{a}_x) < 0$. Correcting δM proportionally to $(a_x - \tilde{a}_x)$, with the same sign, would lead to a decrement of the extended state: however, δM should instead increase to compensate for the greater mass on the vehicle. Thus, the introduction of the sign operator accounts for this issue, an introduces a necessary non-linearity in the correction law.

The considered experiment for the mass estimation is an urban driving one - see Fig. 4b: in said test, only the correction of Eq. (14) is applied.

The results - in case of noisy data and correct center-of-mass - can be appreciated in Fig. 4a: the mass is correctly estimated even by starting from different initial conditions, and the estimate eventually converges to the correct value. Table 4 reports the estimation performance in different conditions: as one can notice, the mass estimate is highly robust both to measurement noise and to imperfect knowledge of the center-of-mass. In the worst case, $rms_M = 0.68$ %: since $\delta M = 355$ kg, the error is smaller than 3 kg.

Figure 5 compares the estimator performance for an snr growing from 5 to 20: we can conclude that for reasonable noise levels, the estimator performance does not drop below the 10%, which was originally set to be our limit.

Finally, note that δM converges to the real value even if we are not correcting δJ_{xx} , δJ_{yy} , δJ_{zz} : this highlights the good decoupling among the estimated variables, without the need for designing a separated model for each of them.

4.3. Yaw inertia and roll inertia estimation

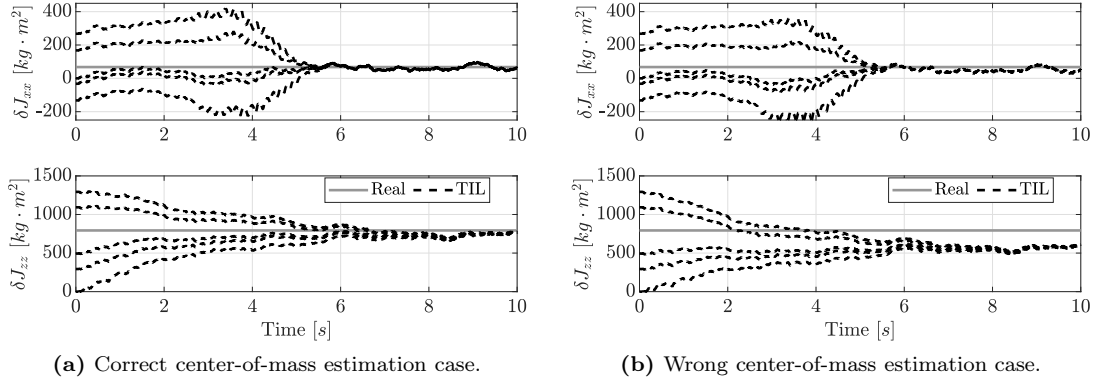


Figure 6. Roll and yaw inertia estimation by means of a swept steer experiment, with noisy measurements. The upper plot depicts the estimated parameters in case the center-of-mass is exactly known, while the lower one depicts them in case the CM is not exactly known.

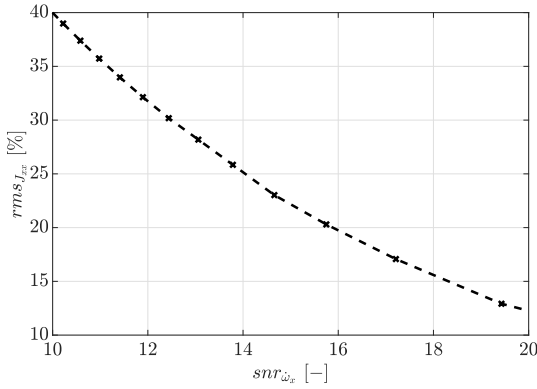


Figure 7. Roll inertia estimation with varying noise levels.

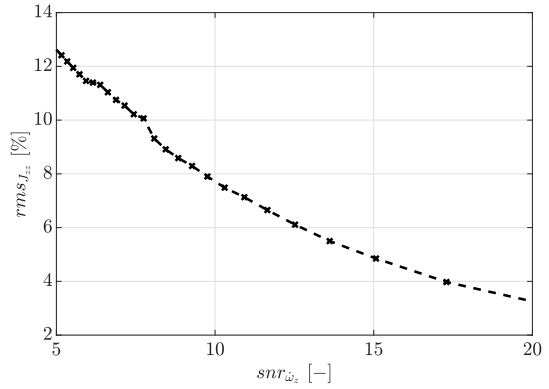


Figure 8. Yaw inertia estimation with varying noise levels.

Roll and yaw inertia can be estimated by exciting lateral dynamics and left-to-right load transfer, which often come together, *e.g.* while negotiating a curve. A proper experiment to estimate both variables at the same time is a swept steer maneuver, at constant speed, from 0 to 4 *Hz*. The non-linear correction law to be applied onto δJ_{xx} and δJ_{zz} follows from what described in Section 4.2 for the mass

$$\begin{aligned} \Delta \delta J_{xx,k_k} &= K_{\dot{\omega}_x - \delta J_{xx}} (\dot{\omega}_{x,k} - \tilde{\omega}_{x,k}) \cdot \text{sgn}(\dot{\omega}_{x,k}), \\ \Delta \delta J_{zz,k_k} &= K_{\dot{\omega}_z - \delta J_{zz}} (\dot{\omega}_{z,k} - \tilde{\omega}_{z,k}) \cdot \text{sgn}(\dot{\omega}_{z,k}). \end{aligned} \quad (15)$$

Where the angular accelerations $\dot{\omega}$ are employed - such signals are easily obtained from the angular rates via differentiation. Note that while estimating J_{xx} and J_{zz} , δM could have been already estimated as described before. Same goes for the center-of-mass. Figure 6a depicts the estimation results in case of noisy measurements, wrong mass estimate, and correct center-of-mass; only corrections in Eq. (15) are applied. The

Table 5. Roll and yaw inertia estimation performance in different conditions.

Test conditions	$rmsJ_{xx}$ [%]	$rmsJ_{zz}$ [%]
Noiseless data ($snr = \infty$); Correct mass; Correct CM.	0.38	0.96
Noiseless data ($snr = \infty$); Wrong mass; Correct CM.	4.22	0.25
Noisy data ($snr = 10$); Correct mass; Correct CM.	23.91	6.18
Noisy data ($snr = 10$); Wrong mass; Correct CM.	26.50	5.38
Noisy data ($snr = 10$); Wrong mass; Wrong CM.	45.43	26.50

estimates converge to the true value, even starting from different initial conditions. On the other hand, Fig. 6b depicts the estimation of the same variable, in case the nominal center-of-mass is kept within the digital twin: as expected, we note a steady-state error in the estimated inertia - mostly noticeable for J_{zz} .

Table 5 quantifies the estimation performance in different cases. One can notice as the error on J_{xx} is generally higher and grows faster as the uncertainty increases. This is easily explained as the nominal value and the variation of J_{xx} are much smaller than for the other inertia. Finally, Fig. 7 and Fig. 8 show the estimator performance when considering different noise levels on the employed measurements. As expected, J_{xx} estimation performance significantly drops, and is never within the 10% limit. On the other hand, J_{zz} estimation shows good performance up to $snr \approx 7.5$, which is a reasonable bound for yaw acceleration noise.

4.4. Pitch inertia estimation

As done above, pitch inertia J_{yy} can be estimated by suitably exciting the corresponding dynamics. The most straightforward way of exciting pitch dynamics is the excitation of the vehicle body with a non-zero road profile: hence, we assume that the vehicle is being driven at constant speed on a paved road. The road profile at front wheels is modeled as [16]

$$z_f = \int_0^t \eta_z, \quad \eta_z \sim WN(0, \sigma_z^2), \quad (16)$$

Where $\sigma_z = 0.01$ m, and WN is the realization of a white noise. Consequently, the profile on the rear wheels is equal to $z_r(t) = z_f(t - v/wb)$, with v the vehicle longitudinal speed, and wb the wheelbase.

The real vehicle, whose load is unknown and has to be estimated, is fed with the generated road profile. The digital twin is then fed with the same road profile. In practice, we are considering that the road profile at the current time is known; this information

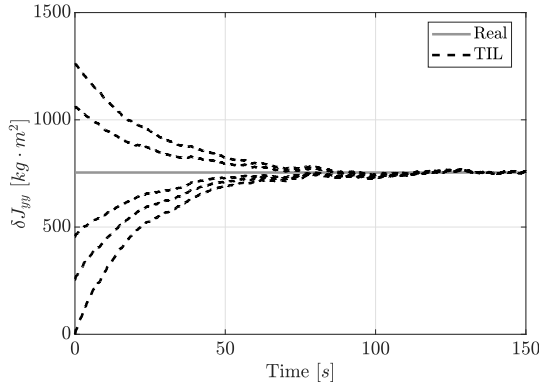


Figure 9. Pitch inertia estimation in case the road is known without uncertainty, with noisy measurements.

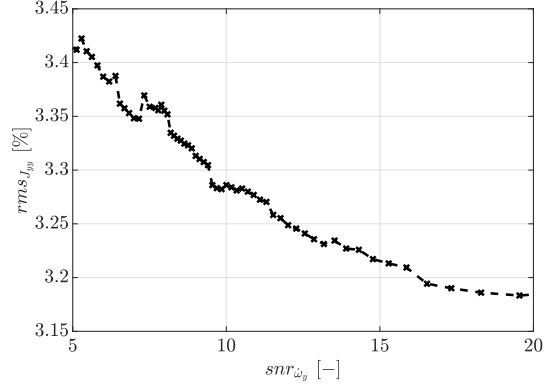
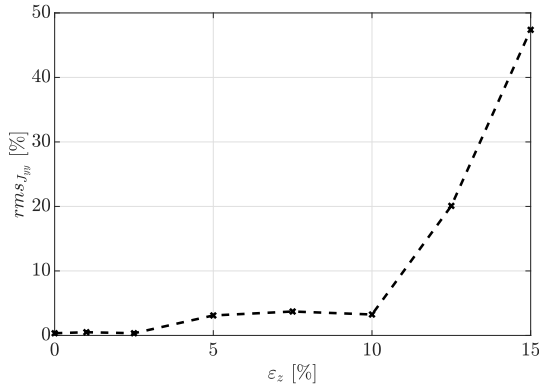
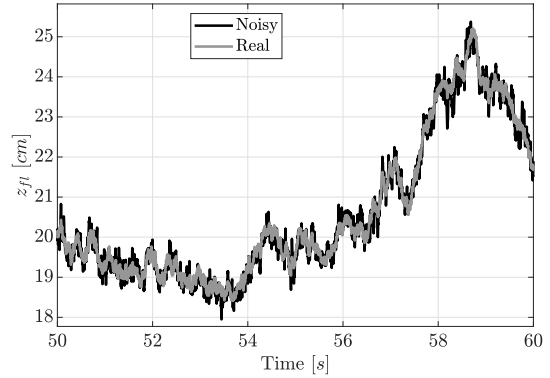


Figure 10. Pitch inertia estimation with varying noise levels. Oscillation in $rms_{\%}$ is intrinsically due to the complex nature of the Twin-in-the-Loop observer.



(a) Sensitivity to J_{yy} estimation error, based on the amount of noise in the road profile.



(b) Noisy versus real road profile, in case $\varepsilon_z = 0.1$.

Figure 11. Analysis on the effect of road profile noise onto the estimation of J_{yy} . (a) shows the sensitivity to J_{yy} estimation error for different noise levels, while (b) compares noisy and real measurements for a specific noise level.

can be easily extracted *e.g.* via Kalman Filtering [11] or sensing devices [19]. To achieve a realistic simulation, we assume the presence of noise in such information

$$z_{f,k}^n = z_{f,k} \cdot u_{z,k}, \quad u_{z,k} \sim \mathcal{U}(1 - \varepsilon_z, 1 + \varepsilon_z). \quad (17)$$

Equation (17) models a multiplicative uniformly distributed noise onto z_f . The correction law to be applied is derived as usual

$$\Delta \delta J_{yy,k_k} = K_{\dot{\omega}_y - \delta J_{yy}} (\dot{\omega}_{y,k} - \tilde{\dot{\omega}}_{y,k}) \cdot \text{sgn}(\dot{\omega}_{y,k}), \quad (18)$$

Where the y -axis angular acceleration $\dot{\omega}_y$ is employed as a measurement. In the following, only correction in Eq. (18) is applied.

As also discussed for roll and yaw inertia, a preliminary estimation of the vehicle mass can yield benefits also to inertia estimation; the same goes for the center-of-mass

position. The inertia estimation - considering noisy measurements - are showed in Fig. 9. The estimate converges to the correct value even by starting from different initial conditions. Also, note that the observer is robust with respect to imperfect knowledge of other inertia parameters J_{xx} and J_{zz} , which are not being corrected.

Then, Table 6 quantifies the estimation performance for different simulation layouts: even in the worst scenario, *i.e.* in case of noisy measurements and road profile information, and wrong knowledge of mass and center-of-mass location, the percentage *rms* settles at $\approx 10\%$.

Finally, Fig. 11a shows the variation of $rms\%$ for increasing road profile noise (ε_z): a significant performance drop arises for $\varepsilon_z > 0.1$.

For a better understanding of the introduced noise level, Fig. 11b depicts the real versus noisy road profiles. The *rms* among the two signals is ≈ 0.2 *cm*, which is comparable to what observed in [11].

Table 6. Pitch inertia estimation performance in different conditions of measurement noise, road profile noise, and with or without the mass estimation.

Test conditions	$rms_{J_{yy}}$ [%]
Noiseless data ($snr = \infty$); Noiseless road profile ($\varepsilon_z = 0$); Correct mass; Correct CM.	0.11
Noiseless data ($snr = \infty$); Noisy road profile ($\varepsilon_z = 0.1$); Correct mass; Correct CM.	3.19
Noisy data ($snr \approx 10$); Noiseless road profile ($\varepsilon_z = 0$); Correct mass; Correct CM	0.33
Noisy data ($snr \approx 10$); Noisy road profile ($\varepsilon_z = 0.1$); Correct mass; Correct CM	3.24
Noisy data ($snr \approx 10$); Noisy road profile ($\varepsilon_z = 0.1$); Wrong mass; Correct CM.	2.38
Noisy data ($snr \approx 10$); Noisy road profile ($\varepsilon_z = 0.1$); Correct mass; Wrong CM.	5.51
Noisy data ($snr \approx 10$); Noisy road profile ($\varepsilon_z = 0.1$); Wrong mass; Wrong CM.	10.20

4.5. Implementation details

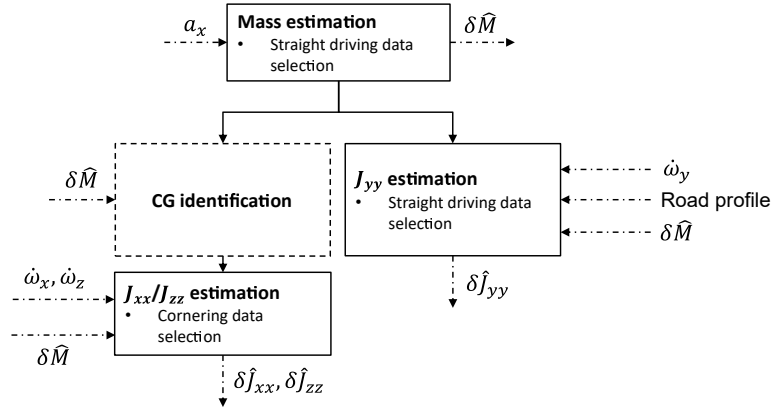


Figure 12. Schematic representation of the operations flow of a possible implementation of the TiL parameters estimator.

In the Sections above, we showed how the TiL approach can properly estimate mass and inertia under different noise and uncertainty conditions; this allowed us to focus on each problem independently. In an actual implementation of the full parameter estimator, one could consider simple logic rules to prioritize estimation of one or more variables. A possibility is that of Fig. 12: the dashed arrows represent outputs/input of a given module of the estimator, while solid arrows describe the flow of operations.

The first stage consists in estimating the vehicle mass. We verified (see Table 4) as this part of the algorithm is extremely robust to knowledge of the center-of-mass and other inertial parameters; hence, this module is the first one to be executed. Estimation during straight driving can be enforced to avoid too highly dynamic conditions: to do so, a simple threshold on vehicle yaw-rate is sufficient. The transition to the next module can be based upon a time threshold: setting a reasonably high threshold ensures that the estimator has converged to the true value when transitioning.

Now, one could estimate the pitch inertia J_{yy} , which has been showed to be robust to center-of-mass knowledge (Table 6); as discussed, this step requires knowledge of the road profile. Also in this case, enforcing straight driving can enhance robustness by avoiding parameter corrections in highly dynamic conditions.

On the other hand, in order to estimate other inertia parameters J_{xx} , J_{zz} we need to know the center-of-mass variation beforehand, so as to have reasonable estimation errors (within the 10 % bound). A suitable estimation procedure can thus be applied to solve for this problem; this enables estimation of roll and yaw inertia, for which a data selection to isolate cornering events is necessary - a threshold on yaw-rate or lateral acceleration solves the last point.

5. Experimental validation

In the following, we test the parameter estimator onto real data. Data has been collected in a proving ground with an high-performance car, and provided by a partner car manufacturer whose name cannot be disclosed for confidentiality reasons.

The vehicle is provided with a set of sensors, yielding the following measurements

- Center-of-mass 3D accelerations and angular rates (IMU);

Parameter						
M_{tot}	J_{xx}	J_{yy}	J_{zz}	d_x [cm]	d_y [cm]	d_z [cm]
1391.29	328.281	1698.21	1864.95	157.14	0	46.22

Table 7. Test vehicle nominal parameters, as modeled on the digital twin.

- Four wheel angular rates (encoders).

For validation purposes, a double antenna GPS is used to measure longitudinal and lateral speed (v_x, v_y). Consequently, the vehicle sideslip β can be computed as $\beta = \text{atan}(v_y/v_x)$. We consider joint estimation of parameters and states: namely, we want to estimate vehicle sideslip and mass. Hence, the augmented state vector is

$$x^{aug} = [x^T \quad \delta M]^T, \quad (19)$$

where $x \in \mathbb{R}^{28 \times 1}$ is the set of simulator states. Measurements vector $y \in \mathbb{R}^{10 \times 1}$ reads

$$y = [a_x \quad a_y \quad a_z \quad \omega_x \quad \omega_y \quad \omega_z \quad \omega_{fl} \quad \omega_{fr} \quad \omega_{rl} \quad \omega_{rr}]^T \quad (20)$$

The most relevant vehicle nominal parameters are collected in Table 7.

5.1. Tuning the TiL observer

Algorithm 1: BO for TiL calibration: pseudo-code

- 1: Select an experiment, consisting of measured states, input, measurements
(x_k, u_k, y_k)
 - 2: Select \mathcal{N} number of total iterations, n_{seed} number of initial points ($n_{seed} < \mathcal{N}$)
 - 3: Evaluate the objective function in n_{seed} random initial points
 - 4: $i \leftarrow n_{seed}$
 - 5: **while** $i < \mathcal{N}$ **do**
 - 6: Update surrogate function $\hat{f}_i(\theta)$
 - 7: Compute acquisition function $a_i(\theta)$
 - 8: Next point to evaluate is $\theta_{i+1} = \arg \min_{\theta} a_i(\theta)$
 - 9: $i \leftarrow i + 1$
 - 10: Evaluate $y_i = f(\theta_i)$
 - 11: **end**
 - 12: Update surrogate function $\hat{f}_{\mathcal{N}}(\theta)$
 - 13: **return** 1) best evaluated point $\bar{\theta} = \arg \min_i f(\theta_i)$
2) best predicted feasible point $\hat{\theta} = \arg \min_{\theta} \hat{f}_{\mathcal{N}}(\theta)$
-

Applying the correction in Eq. (5) with set of states and measurements defined above would yield to state-output mapping matrix $K \in \mathbb{R}^{28 \times 10}$. With regards to the non-linear correction \mathcal{K} , to be applied for the estimation, the expression in Eq. (14) is used. All considered literature solutions rely on Kalman Filters to compute the correction gain to be applied: unfortunately, given that the digital twin is a black-box, we cannot

access its equations, and thus we cannot employ standard techniques - *e.g.* the system linearization, as in Extended Kalman Filter. A data-driven approach is instead here proposed, following what showed in [13]. An optimization procedure is performed based on experimental data: a set of states, driver inputs and measurements is necessary $\langle x_k, u_k, y_k \rangle$. Such procedure calibrates the parameters off-line by minimizing a certain cost function - depending on the estimator objective.

Given that the cost metric to be optimized cannot be written in closed-form - being the simulator equation unknown - we need to rely on a black-box optimizer. These methods suffer of huge scalability problems, and the number of optimization variables shall be reduced as much as possible; this can be enforced by removing variables from the measurements and states vector, reducing the matrix order. Specifically, we consider the following subset of y

$$y_{ss} = [a_x \ a_y \ \omega_y \ \omega_z \ \omega_{fl} \ \omega_{fr} \ \omega_{rl} \ \omega_{rr}]^T. \quad (21)$$

a_z and ω_x have been removed from the set, as we are interested in estimating planar dynamics; on the other hand, one can verify that including the pitch rate ω_y among the measurements can enhance the estimation performance, as the variable is highly related to the road profile - and thus to suspension forces.

The same considerations can be applied to the state vector, thus obtaining a reduced version

$$x_{ss} = [v_x \ v_y \ \omega_y \ \omega_z \ \omega_{fl} \ \omega_{fr} \ \omega_{rl} \ \omega_{rr} \ \delta M]^T. \quad (22)$$

Where the planar velocities allow to algebraically estimate β ; wheel, pitch and yaw angular rates $\omega_{fl,fr,rl,rr}$, ω_y , ω_z are corrected with the corresponding measurements in order to guarantee simulator stability. At this point, mapping matrix has dimensions 9×8 , meaning that 72 parameters shall be calibrated. 72 parameters are still computationally intractable, hence, we promote physics-inspired sparsity in the matrix [1]. In details, we consider the following corrections

- $K_{\omega-\omega}$. Correction onto the wheel angular rates via the corresponding measurements;
- $K_{a_x-v_x}$ and $K_{a_y \rightarrow v_y}$. Correction onto the vehicle longitudinal/lateral speed via the corresponding accelerations;
- $K_{\omega_z-\omega_z}$. Correction onto the yaw rate via the corresponding measurement;
- $K_{\omega_y-\omega_y}$. Correction onto the pitch rate via the corresponding measurement.

Hence, the set of parameters to be tuned reads

$$\theta = [K_{\omega-\omega} \ K_{a_x-v_x} \ K_{a_y \rightarrow v_y} \ K_{\omega_y-\omega_y} \ K_{\omega_z-\omega_z} \ K_{a_x-\delta M}] \quad (23)$$

Where the term $K_{a_x-\delta M}$ is the correction on the vehicle mass; we apply it through the switching law

$$\begin{aligned} \Delta \delta M_k &= K_{a_x-\delta M} \cdot \epsilon(a_{x,k}, \omega_{z,k}) \cdot (a_{x,k} - \tilde{a}_{x,k}), \\ \epsilon &= \begin{cases} 0 & , |\omega_{z,k}| > \bar{\omega}_z, \\ 1 & , \text{sgn}(a_{x,k}) \geq 0 \wedge |\omega_{z,k}| < \bar{\omega}_z, \\ -1 & , \text{sgn}(a_{x,k}) < 0 \wedge |\omega_{z,k}| < \bar{\omega}_z. \end{cases} \end{aligned} \quad (24)$$

Equation (24) is very similar to Eq. (14): however, we introduce a scheduling law based on the yaw-rate ω_z , with $\bar{\omega}_z = 3 \text{ deg/s}$ - as also discussed in Section 4.5 - in order to perform the estimation during straight driving. Now, the optimal observer calibration θ^* can be found by solving the following optimization problem

$$\begin{aligned} & \min_{\theta} J(\theta) \\ & \text{subject to } \theta \subseteq \Theta. \end{aligned} \quad (25)$$

The cost function has to be selected based on the estimation targets. In this case, we have

$$J(\theta) = \sqrt{\frac{1}{N_s} \sum_{i=1}^{N_s} k_{\beta} (\beta_k - \hat{\beta}_k)^2} + \sqrt{\frac{1}{10f_s} \sum_{i=N_s-10f_s}^{N_s} (\delta M_k - \delta \hat{M}_k)^2}. \quad (26)$$

Whereas $k_{\beta} = 100$ accounts for numeric differences among the two cost function terms, and N_s is the number of samples in the experiment. Note that the second term of the cost function weights the mass in the last 10 seconds of experiment. This is because we don't need and don't expect the mass estimation to be as fast as the sideslip one, hence we don't give great relevance to the first part of experiment.

We select Bayesian Optimization (BO) to solve the problem in Eq. (25): BO is a model-free optimizer employed when the cost function to be minimized cannot be written down in form of equation, but we are able to evaluate for some values of θ . A Gaussian Process proxy of the cost function is then found by regression on said points, and used to estimate the global optimum of the problem in Eq. (25). The BO procedure is schematized in Algorithm 1, and more information can be found in one of the many papers about this topic, *e.g.* [3].

5.2. Benchmark estimator

In order to fairly compare the TiL estimator with a benchmark, we build an observer with a double-track planar model as a system replica (see Fig. 13); the same correction architecture as for the TiL, based on constant gains, is retained. This model has been frequently used in the state and parameter estimation literature ([7,27]). Furthermore, we use double-track model for consistency to our previous research on TiL topic [13]. The planar vehicle dynamics are written - in discrete time - as

$$\begin{aligned} v_{x,k+1} &= v_{x,k} + T_s \left(\frac{F_x^T}{M_{tot} + \delta M_k} + v_{y,k} \omega_{z,k} \right), \\ v_{y,k+1} &= v_{y,k} + T_s \left(\frac{F_y^T}{M_{tot} + \delta M_k} - v_{x,k} \omega_{z,k} \right), \\ \omega_{z,k+1} &= \omega_{z,k} + T_s \left(\frac{M_z^T}{J_{zz}} \right), \\ \delta M_{k+1} &= \delta M_k. \end{aligned} \quad (27)$$

Where T_s is the sampling time. The equations are enhanced with the extended state for the mass estimation, δM . The total forces F_x^T , F_y^T and moment M_z^T are respectively

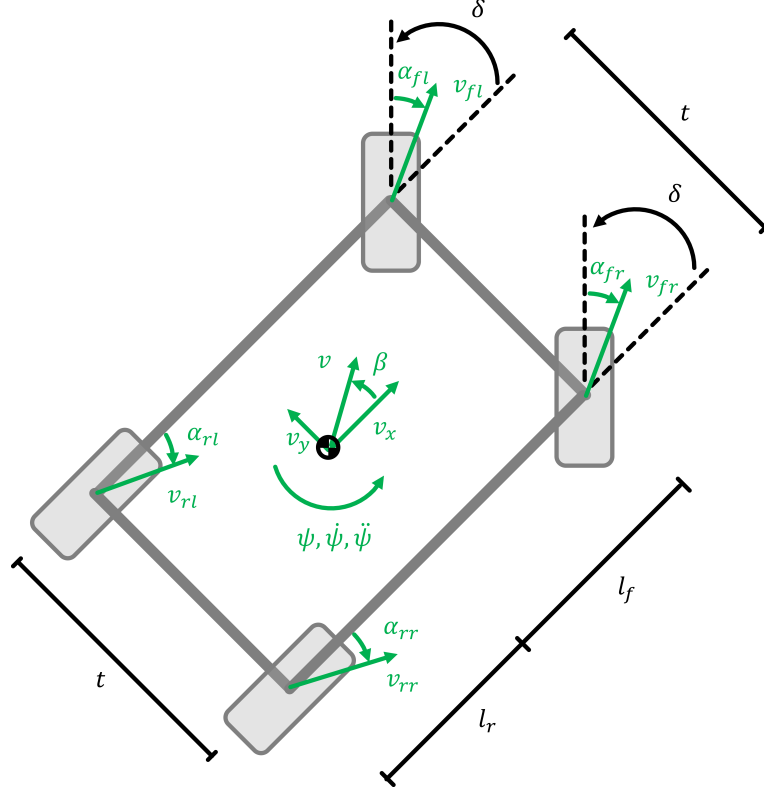


Figure 13. Double-track vehicle model scheme.

written as a function of the tire-road forces

$$\begin{aligned}
F_x^T &= (F_{x,fl} + F_{x,fr}) \cos(\delta) - (F_{y,fl} + F_{y,fr}) \sin(\delta) + \\
&\quad F_{x,rl} + F_{x,rr}, \\
F_y^T &= (F_{x,fl} + F_{x,fr}) \sin(\delta) + (F_{y,fl} + F_{y,fr}) \cos(\delta) + \\
&\quad F_{y,rl} + F_{y,rr}, \\
M_z^T &= l_f (F_{y,fl} + F_{y,fr}) \cos(\delta) + \frac{t}{2} (F_{y,fl} - F_{y,fr}) \sin(\delta) - \\
&\quad \frac{t}{2} (F_{x,fl} - F_{x,fr}) \cos(\delta) + l_r (F_{x,fl} + F_{x,fr}) \sin(\delta) - \\
&\quad l_r (F_{y,rl} + F_{y,rr}) - \frac{t}{2} (F_{x,rl} - F_{x,rr}).
\end{aligned} \tag{28}$$

Where l_f, l_r, t are parameters influenced by the center-of-mass position, which could thus change over time. However, given that the considered case study is a 2-seats car, the expected load variations are not of significant influence to the CM position.

The wheel forces $F_{x,ij}, F_{y,ij}$ are modeled through a simplified Pacejka model [10]

$$\begin{aligned}
F_x^{ij} &= F_{z,ij} D_x \sin(C_x \arctan(B_x \lambda_{ij} - E_x (B_x \lambda_{ij} - \arctan(B_x \lambda_{ij})))), \\
F_y^{ij} &= F_{z,ij} D_y \sin(C_y \arctan(B_y \alpha_{ij} - E_y (B_y \alpha_{ij} - \arctan(B_y \alpha_{ij}))).
\end{aligned} \tag{29}$$

Where F_z^{ij} is the normal force at each wheel; the same can be easily estimated by

using center-of-mass measured accelerations [22]. The wheel longitudinal and lateral slips λ_{ij} , α_{ij} are computed as

$$\begin{aligned}\lambda_{ij} &= \frac{R_{ij}\omega_{ij} - v_{x,ij}}{\max(R_{ij}\omega_{ij}, v_{x,ij})}, \\ \alpha_{ij} &= \arctan(v_y^{ij}/v_x^{ij}).\end{aligned}\tag{30}$$

Where $v_{x,ij}$, $v_{y,ij}$ are obtained from simple kinematic considerations. In principle, one could include the wheel dynamics as in [13], in order to filter the wheel angular rate states. However, since the estimation target is different, and we assume the angular rate measurements to be reliable, we directly consider measured ω_{ij} in Eq. (30). This also avoids us to model the braking and traction torques effect onto the wheels, a potential further source of error. Overall, Eq. (27), Eq. (29), Eq. (30) can be combined in order to obtain the double-track dynamics

$$\begin{aligned}x_{bench,k+1} &= x_{bench,k} + T_s \cdot f_{bench}(x_{bench,k}, u_{bench,k}), \\ y_{bench,k} &= \begin{bmatrix} a_{x,k} \\ a_{y,k} \\ \omega_{z,k} \end{bmatrix} = \begin{bmatrix} \frac{F_x^T}{M_{tot} + \delta M_k} + v_{y,k}\omega_{z,k} \\ \frac{F_y^T}{M_{tot} + \delta M_k} - v_{x,k}\omega_{z,k} \\ \omega_{z,k} \end{bmatrix}.\end{aligned}\tag{31}$$

Whereas $x_{bench} = [v_x \ v_y \ \dot{\psi} \ \delta M]^T \in \mathbb{R}^4$, and $u_{bench,k} = [\delta \ \omega_{fl} \ \omega_{fr} \ \omega_{rl} \ \omega_{rr}] \in \mathbb{R}^5$. f_{bench} is a suitable non-linear function.

We apply on the benchmark estimator the same correction law proposed in Section 2. The correction gains are stored in vector θ_{bench}

$$\theta_{bench} = [K_{a_x - v_x} \ K_{\omega_z - \omega_z} \ K_{a_x - \delta M} \ K_{a_y - v_y}].\tag{32}$$

Bayesian Optimization is employed to tune θ_{bench} , as for the TiL observer.

Remark. *Let us remark that the double-track model - especially the Pacejka parameters - need to be identified based on experimental data: this increases the number of tunable parameters and the calibration complexity of the benchmark. On the other hand, a digital twin of the vehicle is usually already well calibrated, as the same is used for simulation purposes by the car manufacturer. Furthermore, the double-track model is not valid anymore if we want to estimate roll or pitch inertia: we would need to design another ad-hoc model, or to enhance the double-track with non-planar dynamics.*

5.3. Final results

The following results are obtained by testing the TiL estimator and the benchmark defined in Section 5.2. The experiments have been performed on the vehicle having a nominal mass, hence, in order to test the algorithms, we modify the initialization of the estimator internal models, so to have a wrong mass value $\delta_{M,0} = -350 \text{ kg}$.

Figure 14 depicts vehicle speed, steering wheel angle and lateral acceleration in the experiment used for solving optimization problem in Eq. (25) - the test consists in a series of circuit laps. As the reader can note, the experiment is extremely challenging, in that accelerations up to 1.5 g and speed up to 230 km/h are reached.

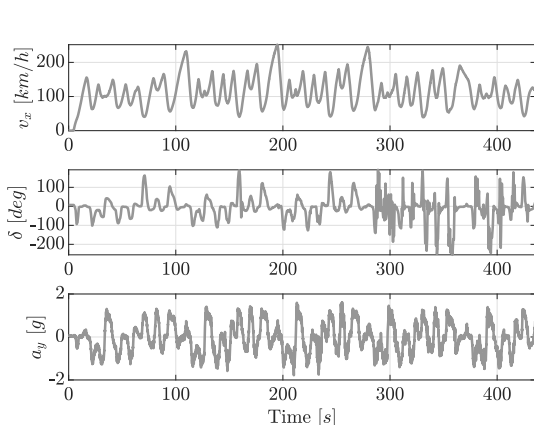


Figure 14. Speed, yaw-rate and lateral acceleration profiles in a series of circuit laps (optimization experiment).

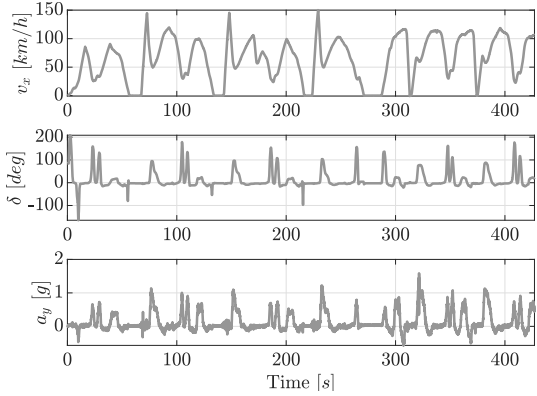


Figure 15. Speed, yaw-rate and lateral acceleration profiles in a series of double-lane-change maneuvers (validation experiment).

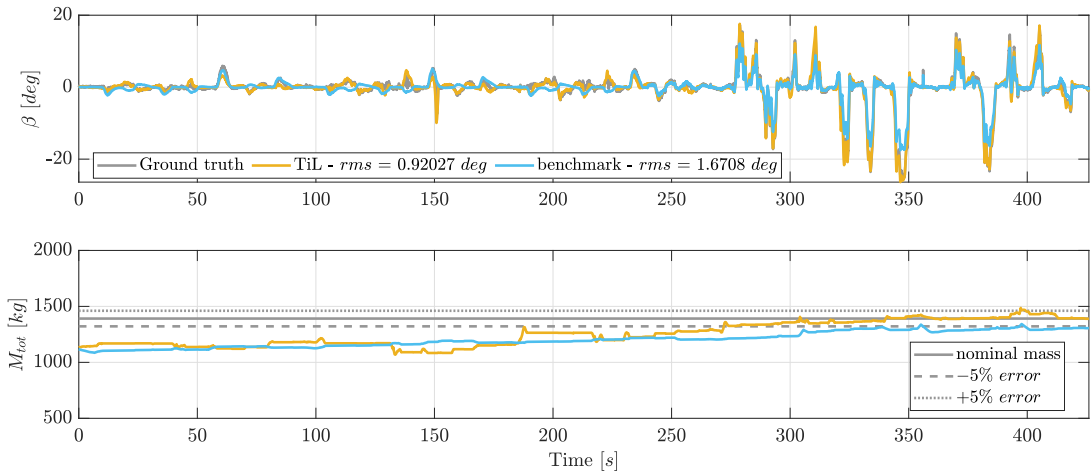


Figure 16. Joint mass and sideslip estimation in a series of circuit laps (optimization experiment). The TiL estimator is compared with a benchmark estimator.

For this test, we apply the BO procedure solving the problem of Eq. (25): the optimal parameters in Table 8 are obtained. The variable bounds can be found via trial-and-error and prior physical knowledge, as discussed in [13]. The estimation results are displayed in Fig. 16. An highlight on the last part of the test is showed in Fig. 17. As one can notice, TiL is able to outperform the double-track based observer both on mass and sideslip estimation. The mass estimate convergence is indeed slower than in the simulation test of Section 4.2: this is however expected, as the real world experiment is significantly more challenging.

Figure 15 shows speed, yaw-rate and lateral acceleration for another experiment, used for validating the estimators - this test consists in a series of double lane change and braking maneuvers, and is thus different in nature from the optimization one. The estimation results are given in Fig. 18. Also in this case, both filters are able to properly estimate the sideslip angle - with a comparable performance. On the other hand, the double-track model is not able to correctly estimate the mass, and seems to be diverging over time.

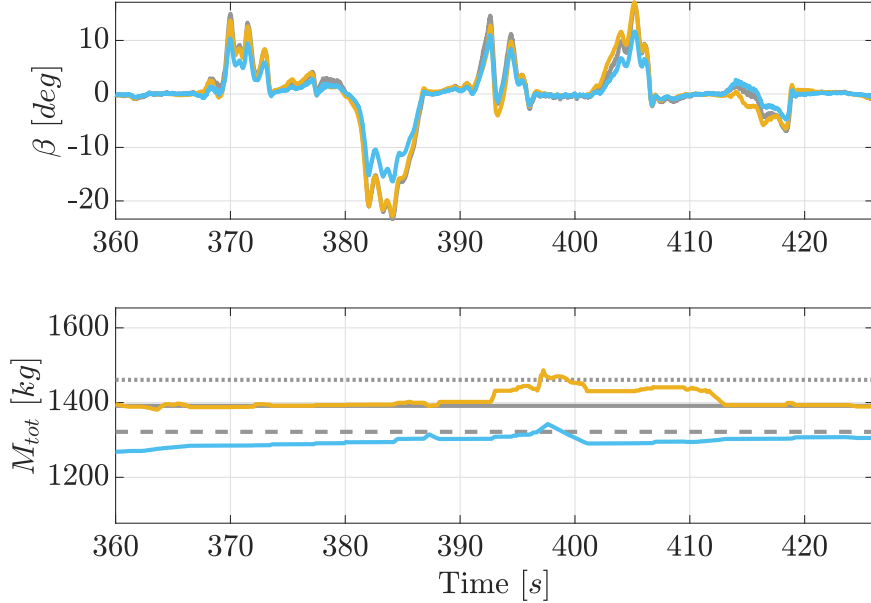


Figure 17. Joint mass and sideslip estimation in a series of circuit laps (optimization experiment). The TiL estimator is compared with a benchmark estimator - highlighted portion.

Parameter	Lower bound	Upper bound	Optimized - TiL	Optimized - bench
$k_{\omega-\omega}$	0	1.5	0.259	/
$k_{a_x-v_x}$	0.01	0.01	$3.287 \cdot 10^{-3}$	$9.282 \cdot 10^{-2}$
$k_{a_y-v_y}$	0.01	0.01	$7.430 \cdot 10^{-2}$	$5.271 \cdot 10^{-2}$
$k_{\omega_y-\omega_y}$	0.2	1.5	0.913	/
$k_{\omega_z-\omega_z}$	0.2	1.5	1.046	0.314
$k_{a_x-\delta M}$	0	1000	248.17	2.06

Table 8. Upper, lower bounds and optimal parameters found for the TiL estimator via BO.

6. Conclusions

In this manuscript, we show that the mass and inertia of a vehicle can be estimated - jointly with classical vehicle dynamics states - via the recently introduced Twin-in-the-Loop filtering approach. The method is validated extensively in simulation, considering independent estimation of each parameter of interest, and performing sensitivity analyses to noise and uncertainty. Then, the TiL estimator is tested against experimental data collected on a high-performance car, showing high performance in joint estimation of mass and sideslip. A comparison with another observer based on state-of-the-art double-track vehicle modelling provides further insights into the potential of the TiL architecture.

Future work will be dedicated to the study of the real-time estimation of the tire-road friction coefficient.

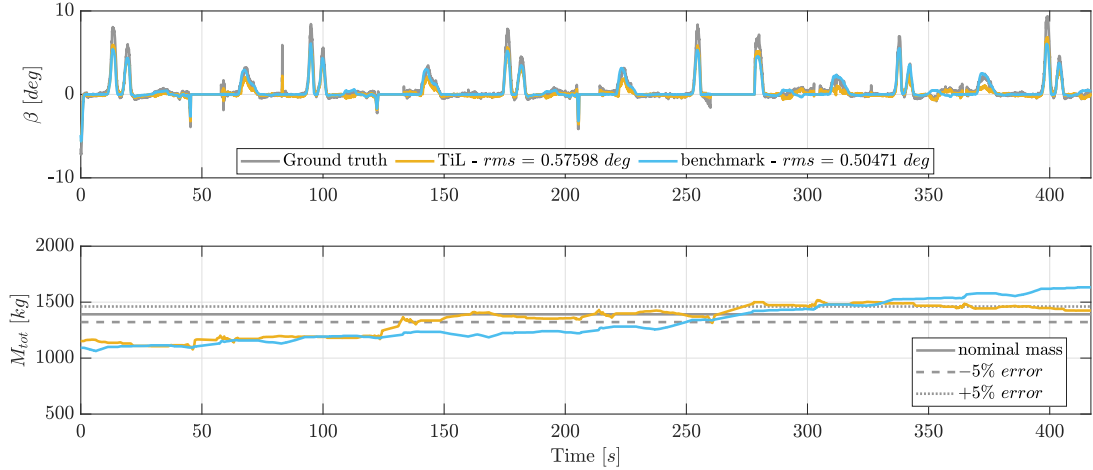


Figure 18. Joint mass and sideslip estimation in a series of circuit laps (validation experiment). The TiL estimator is compared with a benchmark estimator.

Conflicts of Interest

The authors declare no conflict of interest.

References

- [1] Delcaro, G., Dettù, F., Formentin, S., Savaresi, S., 2023. Dealing with the curse of dimensionality in twin-in-the-loop observer design, in: 2023 IFAC World Congress, IFAC.
- [2] Dettù, F., Formentin, S., Savaresi, S.M., 2022. The twin-in-the-loop approach for vehicle dynamics control. arXiv:2209.02263 .
- [3] Gelbart, M.A., Snoek, J., Adams, R.P., 2014. Bayesian optimization with unknown constraints. arXiv preprint arXiv:1403.5607 .
- [4] Gevers, M., 2005. Identification for control: From the early achievements to the revival of experiment design. European journal of control 11, 335–352.
- [5] Gobbi, M., Mastinu, G., Previati, G., 2011. A method for measuring the inertia properties of rigid bodies. Mechanical Systems and Signal Processing 25, 305–318.
- [6] Gong, X., Suh, J., Lin, C., 2020. A novel method for identifying inertial parameters of electric vehicles based on the dual h infinity filter. Vehicle System Dynamics 58, 28–48.
- [7] Hong, S., Lee, C., Borrelli, F., Hedrick, J.K., 2014. A novel approach for vehicle inertial parameter identification using a dual kalman filter. IEEE Transactions on Intelligent Transportation Systems 16, 151–161.
- [8] Huang, X., Wang, J., 2014. Real-time estimation of center of gravity position for lightweight vehicles using combined akf-ekf method. IEEE Transactions on Vehicular Technology 63, 4221–4231. doi:.
- [9] Li, L., Lu, Y., Wang, R., Chen, J., 2016. A three-dimensional dynamics control framework of vehicle lateral stability and rollover prevention via active braking with mpc. IEEE Transactions on Industrial Electronics 64, 3389–3401.
- [10] Pacejka, H., 2005. Tire and vehicle dynamics. Elsevier.
- [11] Qin, Y., Langari, R., Wang, Z., Xiang, C., Dong, M., 2017. Road profile estimation for semi-active suspension using an adaptive kalman filter and an adaptive super-twisting observer, in: 2017 American Control Conference (ACC), IEEE. pp. 973–978.
- [12] Reina, G., Paiano, M., Blanco-Claraco, J.L., 2017. Vehicle parameter estimation using a model-based estimator. Mechanical Systems and Signal Processing 87, 227–241.

- [13] Riva, G., Formentin, S., Corno, M., Savaresi, S.M., 2022. Twin-in-the-loop state estimation for vehicle dynamics control: theory and experiments. arXiv:2204.06259 .
- [14] Rodríguez, A.J., Sanjurjo, E., Pastorino, R., Naya, M.Á., 2021. State, parameter and input observers based on multibody models and kalman filters for vehicle dynamics. *Mechanical Systems and Signal Processing* 155, 107544.
- [15] Rozyn, M., Zhang, N., 2010. A method for estimation of vehicle inertial parameters. *Vehicle system dynamics* 48, 547–565.
- [16] Savaresi, S.M., Poussot-Vassal, C., Spelta, C., Sename, O., Dugard, L., 2010. Semi-active suspension control design for vehicles. Elsevier.
- [17] Solmaz, S., Akar, M., Shorten, R., Kalkkuhl, J., 2008. Real-time multiple-model estimation of centre of gravity position in automotive vehicles. *Vehicle System Dynamics* 46, 763–788.
- [18] Tavernini, D., Vacca, F., Metzler, M., Savitski, D., Ivanov, V., Gruber, P., Hartavi, A.E., Dhaens, M., Sorniotti, A., 2020. An explicit nonlinear model predictive abs controller for electro-hydraulic braking systems. *IEEE Transactions on Industrial Electronics* 67, 3990–4001. doi:.
- [19] Theunissen, J., Sorniotti, A., Gruber, P., Fallah, S., Ricco, M., Kvasnica, M., Dhaens, M., 2020. Regionless explicit model predictive control of active suspension systems with preview. *IEEE Transactions on Industrial Electronics* 67, 4877–4888.
- [20] Thornton, S., Marion, J., 2004. *Classical Dynamics of Particles and Systems*. Brooks/Cole.
- [21] VI-Grade, 2022. Vi-carrealtime. <https://www.vi-grade.com/en/products/vi-carrealtime/>. [Online; accessed 23-March-2022].
- [22] Viehweger, M., Vasseur, C., van Aalst, S., Acosta, M., Regolin, E., Alatorre, A., Desmet, W., Naets, F., Ivanov, V., Ferrara, A., et al., 2021. Vehicle state and tyre force estimation: demonstrations and guidelines. *Vehicle system dynamics* 59, 675–702.
- [23] Wang, C., Wang, Z., Zhang, L., Cao, D., Dorrell, D.G., 2020. A vehicle rollover evaluation system based on enabling state and parameter estimation. *IEEE Transactions on Industrial Informatics* 17, 4003–4013.
- [24] Wenzel, T.A., Burnham, K., Blundell, M., Williams, R., 2006. Dual extended kalman filter for vehicle state and parameter estimation. *Vehicle system dynamics* 44, 153–171.
- [25] Wielitzka, M., Dagen, M., Ortmaier, T., 2015. Joint unscented kalman filter for state and parameter estimation in vehicle dynamics, in: 2015 IEEE Conference on Control Applications (CCA), IEEE. pp. 1945–1950.
- [26] Yang, S., Liu, T., Cheng, Y., 2008. Automatic measurement of payload for heavy vehicles using strain gages. *Measurement* 41, 491–502.
- [27] Zhu, J., Wang, Z., Zhang, L., Zhang, W., 2019. State and parameter estimation based on a modified particle filter for an in-wheel-motor-drive electric vehicle. *Mechanism and Machine Theory* 133, 606–624.